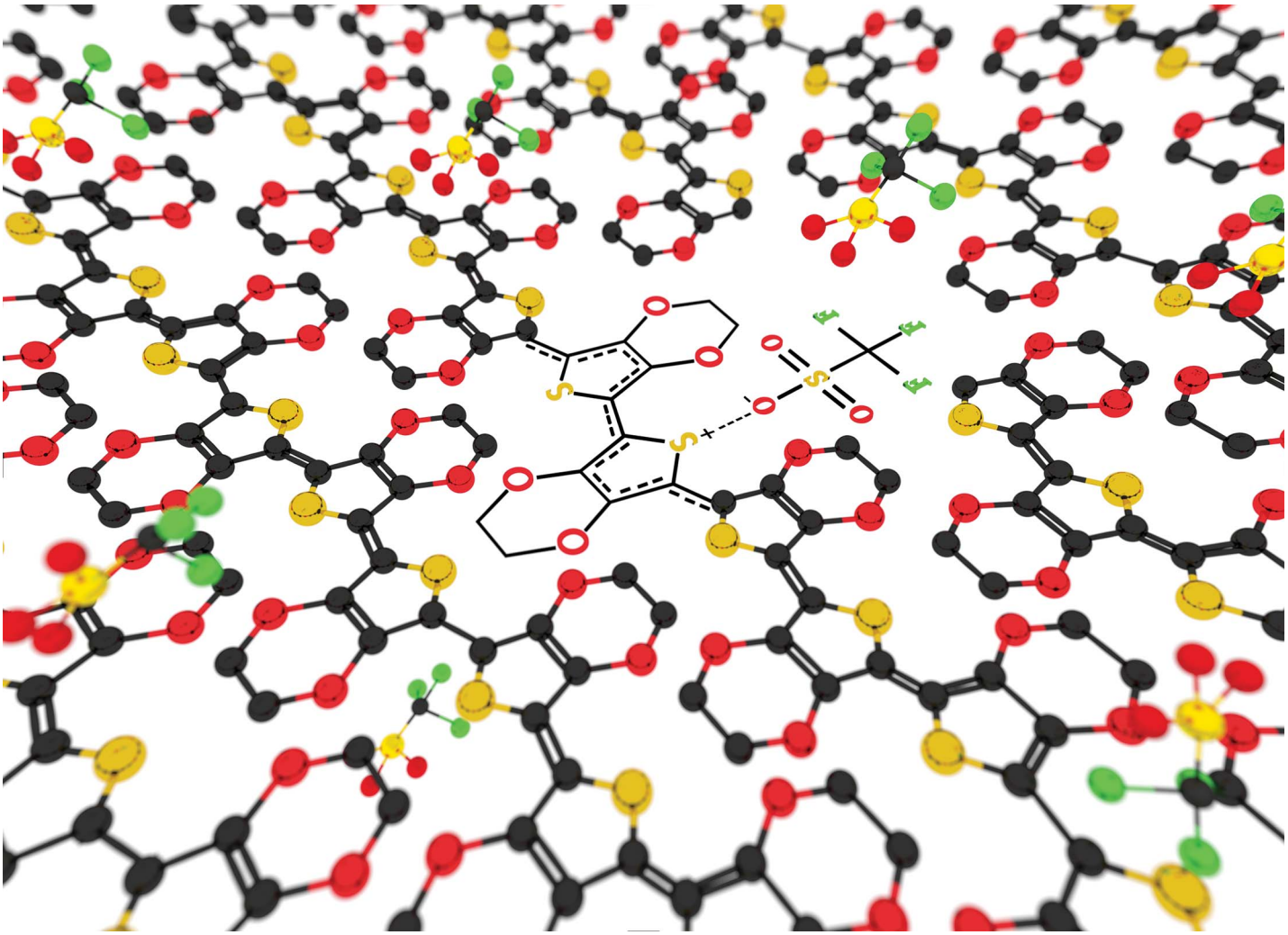

Highlighting an experimental and theoretical study of poly(3,4-ethylenedioxythiophene) with a trifluoromethane sulfonate dopant for use as a transparent conductor overseen by Prof. Xavier Crispin at Linkoping University in Sweden.

Vapor phase synthesized poly(3,4-ethylenedioxythiophene)-trifluoromethanesulfonate as a transparent conductor material

Electrical conductivity values as high as 4500 S cm^{-1} were obtained for the PEDOT thin films after an acid treatment with transparency >85% (at 550 nm).

As featured in:

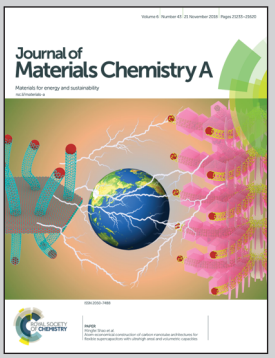

See Xavier Crispin *et al.*,
J. Mater. Chem. A, 2018, **6**, 21304.

ROYAL SOCIETY OF CHEMISTRY

rsc.li/materials-a

Registered charity number: 207890

Journal of Materials Chemistry A

PAPER

View Article Online
View Journal | View Issue

Cite this: *J. Mater. Chem. A*, 2018, **6**, 21304

Vapor phase synthesized poly(3,4-ethylenedioxythiophene)-trifluoromethanesulfonate as a transparent conductor material†

Robert Brooke,[a] Juan Felipe Franco-Gonzalez,[a] Kosala Wijeratne,[a] Eleni Pavlopoulou,[b] Daniela Galliani,[c] Xianjie Liu,[d] Roudabeh Valiollahi,[a] Igor V. Zozoulenko[a] and Xavier Crispin*[a]

Received 21st May 2018
Accepted 6th August 2018

DOI: 10.1039/c8ta04744h

rsc.li/materials-a

Inorganic transparent conductive oxides have dominated the market as transparent electrodes due to their high conductivity and transparency. Here, we report the fabrication and optimization of the synthesis of poly(3,4-ethylenedioxythiophene) trifluoromethanesulfonate *via* vapor phase polymerization for the potential replacement of such inorganic materials. The parameters and conditions of the polymerization were investigated and an electrical conductivity of 3800 S cm^{-1} and 4500 S cm^{-1} after acid treatment were obtained while maintaining an absorbance similar to that of commercial indium tin oxide. This increase in electrical conductivity was rationalized experimentally and theoretically to an increase in the oxidation level and a higher order of crystallinity which does not disrupt the π−π stacking of PEDOT chains.

Introduction

The field of electronic devices is fast approaching the realms of flexible electronics with plastic substrates and developments in material components. However, within the sub-field of opto-electronic devices, commercial transparent conductive materials still rely on indium and other metallic elements. Among the many alternatives explored such as graphene and carbon nanotubes, conductive polymers (CPs) possess certain attributes that may surpass other material pathways. The use of CPs allows more abundant atomic elements to be incorporated instead of rare species such as indium. The synthesis of CPs is not energy intensive, typically at low temperature in solution (<150 °C), and their processing can be through low-cost solution processing techniques, key features for making these technologies economically viable.[1,2] Unfortunately, CPs have certain drawbacks that restrict their uptake commercially. Stability and low electrical conductivity are among the most limiting drawbacks when considering the commercialization of CPs. Researchers have therefore explored methods to improve these limiting properties.[3,4] Within the CP field, arguably the most applicable for commercialization as a transparent conductor is poly(3,4-ethylenedioxythiopene) (PEDOT).[5–7] PEDOT's popularity in opto-electronics is due to its relative stability in ambient conditions and its relatively high electrical conductivity in its oxidised form or doped form (compared to other CPs).[4,7] Doping takes place typically during the synthesis through an oxidizing agent of a certain strength and PEDOT chains become positively charged. Negatively charged counterions are thus necessary to stabilize and keep the material electroneutral. Typical molecular anions include poly(styrene sulfonate), *para*-toluene sulfonate and many others (Fig. 1a and b). While many factors affect the attributes of the PEDOT, the choice of counterions (both during synthesis and post-synthesis) is considered a major factor determining the properties of the resultant CP.[8]

In certain synthesis techniques, such as chemical polymerization and vapour phase polymerization (VPP), the anions

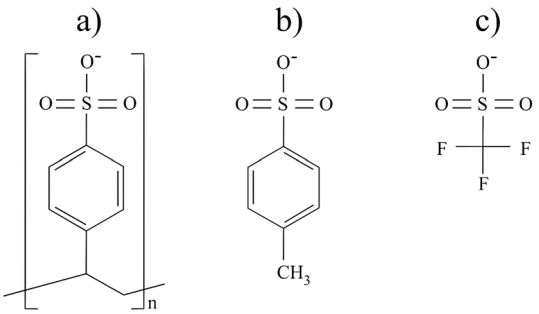

Fig. 1 Chemical structure of common counter ions (a) poly(styrene sulfonate), (b) *para*-toluene sulfonate and the counterion used in this work, (c) trifluoromethane sulfonate.

[a]*Linköping University, Department of Science and Technology, Laboratory of Organic Electronics, SE-601 74 Norrköping, Sweden. E-mail: Xavier.crispin@liu.se*
[b]*Bordeaux INP, Université de Bordeaux, CNRS, LCPO UMR 5629, 33600 Pessac, France*
[c]*University of Milano-Bicocca, Department of Material Science, via R. Cozzi 55, I-20125 Milano, Italy*
[d]*Linköping University, Department of Physics, Chemistry and Biology, Linköping, Sweden*

† Electronic supplementary information (ESI) available. See DOI: 10.1039/c8ta04744h

present in the oxidant employed to polymerise the monomers become the counterions of PEDOT.[2,4] Therefore, the use of the oxidant iron(III) trifluoromethane sulfonate ($Fe(OTf)_3$) (Fig. 1c) allows the polymerization to take place and results in the PEDOT:OTf.[9]

The fluorinated iron oxidant, $Fe(OTf)_3$, has previously been employed for the polymerization of EDOT through a conventional chemical pathway resulting in improvements in electrical conductivity.[9,10] However, it was unclear what scale and appearance the PEDOT films took on and if the films are usable for CP applications such as replacement of indium tin oxide for transparent electrodes.

Herein we present VPP of EDOT using $Fe(OTf)_3$ as the oxidant species to create highly conductive thin films in practical form. The VPP parameters are investigated to find optimised conditions in terms of optical transparency and electrical conductivity. Pristine and acid treated PEDOT:OTf films were investigated in order to observe the increase in conductivity. We then compare our optimized PEDOT:OTf films to commercially available ITO and PEDOT:Tos films.

Computational modelling is essential for a molecular understanding of conducting polymer characterization. Recently, some of the present authors reported molecular dynamics (MD) simulations of morphology and crystallization of doped PEDOT:Tos[11] and doped PEDOT with different counterions, where their effect on the electronic, structural and morphological properties of the polymer has been studied.[12] In the present study the experimental characterization of PEDOT:OTf films has been combined with the theoretical modelling of the material morphology and X-ray diffraction pattern. This made it possible to provide a theoretical understanding of the pristine and acid treated films on the nanoscale, to determine the factors leading to the increase in conductivity, and to provide a theoretical explanation of the experimental Grazing Incidence Wide Angle X-ray Scattering (GIWAXS) measurements.

Experimental

Iron(III) trifluoromethanesulfonate ($Fe(OTf)_3$) was purchased from Alfa Aesar. 3,4-ethylenedioxythiophene (EDOT) and triblock copolymer poly(ethylene glycol)-*block*-poly(propylene glycol)-*block*-poly(ethylene glycol) (PEG-PPG-PEG, 5800 g mol^{-1}) were purchased from Sigma Aldrich. All chemicals were used as received without further purification.

PEDOT:OTf thin films were synthesized similar to those reported previously.[4,13] The oxidant solution components were varied in order to optimise the process with the general parameters of 3 wt% $Fe(OTf)_3$, 20 wt% PEG-PPG-PEG dissolved in ethanol with a polymerization time of 30 minutes and polymerization temperature set to 60 °C while one parameter (oxidant concentration, solvent, polymerization time or temperature) was altered. The role of the PEG-PPG-PEG copolymer has been investigated previously and can be found here.[14] The oxidant solution was spin coated on glass substrates (with a gold electrode for electrical and thermoelectrical characterization) at 1500 rpm for 30 seconds. The oxidant coated substrates were placed on a 70 °C hot plate for 30 seconds before being placed immediately in a VPP chamber and placed under vacuum with the monomer heated to 60 °C. After 30 minutes the films were removed and washed with ethanol and air dried with nitrogen before analysis.

PEDOT:Tos films were synthesized for comparison in a similar procedure to that mentioned above albeit with a different oxidant mixture. The PEDOT:Tos oxidant mixture consisted of 12 wt% iron(III) *para*-toluene sulfonate ($Fe(Tos)_3$) and 22 wt% PEG-PPG-PEG dissolved in ethanol.

Acid treatment consisted of soaking the films for 10 minutes in 1 M H_2SO_4 followed by heating at 100 °C for 10 minutes.

Characterization

Conductivity measurements were achieved using gold electrodes in a four-probe configuration patterned onto glass substrates using thermal evaporation. The area between the inner electrodes was 1 × 1 cm^2. The sheet resistance (R_s) of the samples was measured using a source meter (Keithley 2400) in four-wire sense mode. The conductivity (σ) was calculated using eqn (1):

$$\sigma = \frac{1}{R_s t} \quad (1)$$

where t is the sample thickness, σ is the conductivity and R_s is the sheet resistance.

The film thickness was measured using atomic force microscopy (AFM). AFM images were obtained in tapping mode using a Veeco Dimension 3100. The morphological images and thickness measurements were analyzed using Gwyddion and WSxM 4.0 software.[15] Ultraviolet-visible (UV-Vis) absorption spectra were acquired (Lambda 900 spectrometer, PerkinElmer). The spectra were recorded between 350 and 1050 nm. Extinction coefficients were calculated using the Beer–Lambert law, eqn (2):

$$\alpha = A \times t \quad (2)$$

X-ray photoemission experiments were performed using a Scienta ESCA 200 spectrometer in an ultrahigh vacuum with a base pressure of 10^{-10} mbar. The measurement chamber was equipped with a monochromatic Al Kα X-ray source providing photons with 1486.6 eV and the conditions were set so that the full width at half maximum of the clean Au 4f7/2 line was 0.65 eV. All spectra were measured at a photoelectron takeoff angle of 0° (normal emission).

The electrochemical setup consisted of a three electrode configuration with a Ag/AgCl (3 M KCl) reference electrode, a platinum mesh electrode as the counter electrode and pristine PEDOT/acid treated PEDOT as the working electrode. Cyclic voltammetry was performed in an aqueous solution of 1 M KCl as the electrolyte at room temperature with a computer controlled potentiostat (SP200, BioLogic) using 85% of Ohmic drop correction (determined by impedance measurements at 50 kHz and 20 mV amplitude prior to each voltammetry measurements).

Molecular dynamics simulations

The molecular dynamics (MD) simulations described in this work were performed using the LAMMPS software package.[16]

The parameters for PEDOT, OTf, HSO_4^- and ethanol were taken from the General AMBER Force Field (GAFF)[17] as implemented in the moltemplate code.[18] Water molecules were represented by the SPC/E model.[19] The Lennard-Jones (LJ) and coulombic interactions were cut off at 1.2 nm with a neighbor list updated at every step and a cut-off at 1.4 nm. The simulation setups correspond to two different systems: pristine and acid treated systems. The pristine setup corresponds to PEDOT:OTf where ethanol is the solvent. The acid treated setup corresponds to PEDOT:HSO_4^- where the solvent is water. These setups include 40 PEDOT chains with the oxidation levels corresponding to those measured by XPS as reported below: 25% and 32% for pristine and acid treated systems, respectively. We considered the chain length of PEDOT as 12 repeated monomer units. The chain length of PEDOT is not exactly known experimentally but is estimated to be in the range of 6–20 monomer units depending on the synthesis method employed.[20] Finally, we note that for a similar system, PEDOT:Tos, the simulated morphology was shown to be rather insensitive to the chain length.[11] Partial charges on each atom of PEDOT, OTf, HSO_4^- and ethanol molecules were calculated using first-principles density-functional theory (DFT) functional WB97XD[21] with the 6-31+g(d) basis set[22] as implemented in Gaussian 09, revision E.01 2009.[23] The partial charge per atom was taken from the fitting to electrostatic potential (ESP) population analysis[24] as implemented in Gaussian suite. The corresponding numbers of OTf and HSO_4^- to balance the charges of the system were considered in a proper proportion as measured by XPS.

In our simulations, we start from a diluted polymeric solution and remove the solvent in several steps until the X-ray pattern of the simulated systems coincides with the corresponding experimental GIWAXS pattern. This is due to the fact that the solvent content of the films is not known and the X-ray diffraction is sensitive to the amount of solvent as demonstrated by the authors for similar PEDOT related systems.[11,25] Therefore, the box is initially solvated with 6744 ethanol molecules and 19 844 water molecules for the pristine and acid treated systems, respectively. The system was then minimized and equilibrated by a 2 ns run of isobaric–isothermal npT using both a Nose–Hoover thermostat and barostat.[26] Then, a production run of 50 ns of a canonical nVT ensemble using the Nose–Hoover thermostat is performed. The time integration method of Verlet[27] is applied. Then, the solvent was consecutively removed in 8 steps: the solvent concentration was reduced, approximately, from 82% wt (initial solution) to 79 wt%, 76 wt%, 73 wt%, 65 wt%, 58 wt%, 48 wt%, 31 wt% and finally 0 wt% (*i.e.* a dry phase). The system was equilibrated in each step using an npT ensemble for a 10 ns run with both the Nose–Hoover barostat and thermostat with corresponding adjustment (decreasing) of its volume. Also, at each step, as a standard protocol, the simulations were performed until the potential energy of the system reached saturation. In all simulations, the temperature was kept close to the boiling point of the solvent: 69.9 °C and 100 °C for ethanol and water, respectively. X-ray diffraction patterns were simulated as described by Coleman *et al.*[28] and implemented in LAMMPS suite.

GIWAXS

Grazing Incidence Wide Angle X-ray Scattering (GIWAXS) experiments were performed on the Dutch-Belgian Beamline (DUBBLE CRG), station BM26B, at the European Synchrotron Radiation Facility (ESRF), Grenoble, France.[29] The wavelength of the X-rays, λ, was 1.033 Å while the sample-to-detector distance and the angle of incidence, α_i, were set at 8.08 cm and 0.15°, respectively. Details on data treatment, data corrections and scattering vector (q, q_r, and q_z) definitions can be found elsewhere.[25]

Results and discussion

Synthesis of highly conductive PEDOT

Vapor phase polymerization is a synthetic route where a solution of the oxidant $Fe(OTf)_3$ and the copolymer PEG-PPG-PEG dissolved in an alcohol are spin-coated on an insulating substrate. The thin film of the composite PEG-PPG-PEG/$Fe(OTf)_3$ is then exposed to EDOT vapor for a certain time, temperature and pressure. Once the PEDOT:OTf film is formed, the remaining iron salt, $Fe(OTf)_2$ and unreacted $Fe(OTf)_3$ are dissolved in the cleaning procedure. The composition of the oxidant solution is one of the key ingredient to optimize the electrical conductivity of the resulting PEDOT:OTf. In general, an increased oxidant concentration produces a thicker layer of CP in VPP due to more nucleation sites and the monomer having more oxidant available for the polymerization.[2,30] However, no report has yet investigated the effect of the $Fe(OTf)_3$ concentration on the resulting optical and electrical properties of the CP. Many reports have stated that a slower polymerization rate in VPP provides the CP chains a suitable time in order to stack and orient themselves optimally, permitting favourable electrical properties.[5,6,8] Therefore, one may assume that a lower oxidant concentration may result in better electrical conductivity. Although if the polymerization becomes too slow the CP film may not survive the washing step subsequent to the VPP step.

Fig. 2a displays the electrical conductivity and absorption spectrum for various concentrations of oxidant in ethanol. As expected the larger the oxidant concentration, the thicker the film as indicated by the absorbance (3 wt% = 30.7 nm, α = 0.088, 6 wt% = 90.2 nm, α = 0.14, 12 wt% = 206.2 nm, α = 0.32). The lowest concentration of 3 wt% $Fe(OTf)_3$ leads to the highest conductivity and lowest absorbance spectra in the visible region. With an acid treatment (1 M H_2SO_4, see the Experimental section for details), the conductivity of the 3 wt% sample is increased to 4471 S cm^{-1} with an absorbance below 0.2 (the absorbance spectra for the oxidant concentration and solvent variation of the acid treated films are shown in Fig. SI1 and SI2†), showing its potential as a transparent conductor material. Indeed, ITO has an electrical conductivity of 4000 S cm^{-1} and an absorbance of <0.1 at 550 nm in the visible region.[31,32] The surface properties were also investigated (Fig. SI3†) and a RMS roughness of 4.89 nm for the 3 wt% sample over a 3 × 3 μm^2 area was obtained showing that the film is smooth; which is a prerequisite for opto-electrical applications, thus avoiding

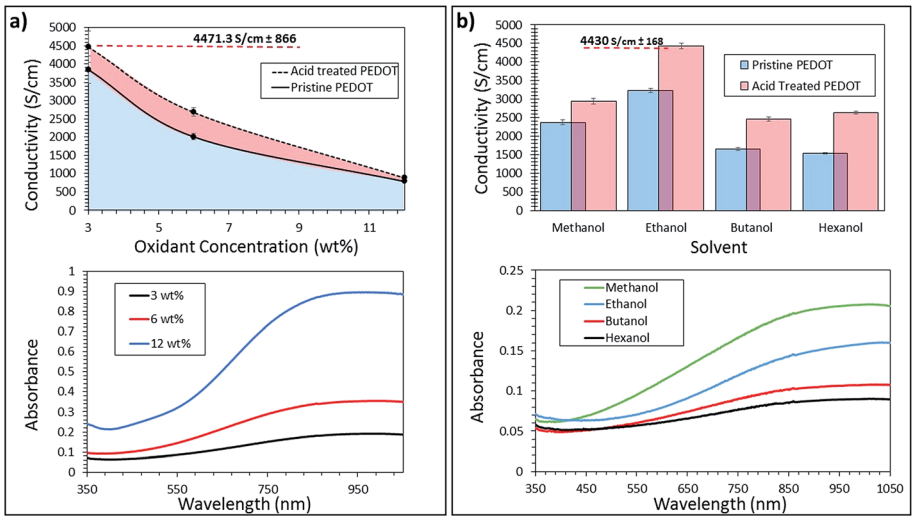

Fig. 2 VPP parameter investigation. (a) $Fe(OTf)_3$ concentration variation and its effects on electrical conductivity before and after acid treatment of PEDOT:OTf, together with UV-Vis spectra of the pristine films. The oxidant was composed of 20 wt% PEG-PPG-PEG in ethanol with various $Fe(OTf)_3$ amounts. (b) Alcohol based solvent variation and the effects on electrical conductivity before and after acid treatment of PEDOT:OTf, together with UV-Vis spectra of the pristine films. The oxidant was composed of 3 wt% $Fe(OTf)_3$ and 20 wt% PEG-PPG-PEG in various alcohol based solvents. The polymerization temperature was set at 60 °C and polymerization was performed for 30 minutes.

short circuits between thin semiconducting films upon deposition of the top electrode in light emitting diodes or solar cells.

The chemical nature of the solvent is another important parameter to control since it affects both the wettability of the oxidant solution on a substrate and the morphology of the PEG-PPG-PEG/$Fe(OTf)_3$ composite film. A previous report[10] investigating $Fe(OTf)_3$ employed mixtures of ethanol and various other organic solvents such as THF, DMF, DMSO and NMP; however, the mixtures of these solvents with ethanol and the neat organic solvents either did not dissolve the oxidant or resulted in poor wettability. A separate report investigated the effect of various organic solvent additions to the $Fe(Tos)_3$ oxidant solution, but none outperformed the ethanol solution.[33] Alcohol based solvents have been used extensively in the VPP of EDOT[3,4,34,35] and several of them were trialled for the best electrical and optical properties of PEDOT. Similar to the studies on PEDOT:Tos, we show that ethanol provides the highest electrical conductivity for PEDOT:Tof before (3250 ± 122 S cm^{-1}) and after acid treatment (4430 ± 168 S cm^{-1}) (Fig. 2b). The surface properties were acceptable for all solvents with only methanol producing a RMS roughness of above 5 nm (Fig. SI4†). The surface roughness of the glass substrates was measured to be an average of 3.1 nm (Fig. SI5†) which would influence the overall surface roughness. The surface roughness values for the PEDOT samples which still possess an acceptable value for organic electronics could be improved to make this material even more suitable as an electrode material. Interestingly, we see a correlation between the thickness of the film, proportional to the absorbance in the spectrum, and the ebullition point of the alcohols (methanol: 65 °C; ethanol: 78 °C; butanol: 118 °C; hexanol: 157 °C). This can be attributed to the presence of the remaining solvent trapped in the PEG-PPG-PEG/$Fe(OTf)_3$ films. Therefore, during the polymerization, the monomer vapour does not react with as many oxidant molecules due to the presence of alcohol molecules still remaining in the oxidant film. The use of the longest alcohol trialled, hexanol, resulted in a PEDOT film of the lowest absorbance (Fig. 2b) with an average thickness of 15.8 nm. This sample was not the most impressive in terms of electrical conductivity (2655 S cm^{-1} after acid treatment compared to 4011 S cm^{-1} for ethanol) suggesting the importance of the removal of absorbed alcohol molecules prior to polymerization or the negative effect of the high boiling point solvent on the morphology of the oxidant films.

Both polymerization time and temperature were also investigated and the results can be seen in the ESI (Fig. SI6 and SI7†). From the electrical conductivity and general appearance of the PEDOT films an optimal polymerization time of 10 minutes with a polymerization temperature of 30 °C was set for all future experiments. This optimization is most likely a result of the polymerization progressing slowly enough to provide the growing polymer chains time to align and stack in an optimised orientation while still being able to endure the washing step. The use of vacuum was also shown to be of utmost importance with a dramatic reduction in electrical conductivity from 4000 S cm^{-1} to 1000 S cm^{-1} upon pressure increase to atmospheric pressure (Fig. SI8†). It is thought that the greater control of the water content under vacuum conditions is responsible for the high conductivity. The reproducibility of the optimised conditions is acceptable with only a minimal variation between samples (Fig. SI9†) and between batches (± 225 S cm^{-1} maximum) (Fig. SI10†) giving an electrical conductivity of approximately 4500 S cm^{-1}.

The optimized PEDOT:OTf has enormous potential as a transparent conductor with its high conductivity and high transparency within the visible spectrum. Comparing the new PEDOT:OTf shown in this report to other transparent electrode materials such as PEDOT:Tos and ITO coated glass substrates highlights the potential of the PEDOT:OTf. In terms of

conductivity the PEDOT:OTf (4500 S cm^{-1}) is superior to all the materials, even the commercial ITO substrate (4000 S cm^{-1}[31,32]) (the highest recorded ITO conductivity may be superior but not commercially available ITO). The optical spectra of the PEDOT:OTf are only slightly lower than those of ITO across the measured region (Fig. 3b) and higher within the UV region. Fig. 3a shows the compared materials and their transparency over the Linkoping University logo. Absorbance and normalized absorbance to material thickness can be found in the ESI (Fig. SI11†).

Stability investigation

Throughout this report the properties of the PEDOT films have been presented before and after acid treatment. One question that has been foreseen is the stability of the films after the acid treatment. Acid treatments are thought to modify polymer chains which may lead to faster degradation under ambient conditions. Interestingly, the stability with regard to electrical stability under ambient conditions over time was good with only a small increase of resistance over 200 hours and the acid treated films follow the same trend as that of the pristine films (Fig. 4a). Furthermore, after a series of redox cycles the acid treated PEDOT:OTf and the pristine film were equally stable over 1000 cycles (Fig. 4b). There were also no observable changes in the morphology of the films before and after the acid treatment as seen in Fig. SI12.† The optical properties were also examined over time and no degradation was observed over 150 hours in the ambient atmosphere. The acid treated film has a lower absorption at 900 nm than the pristine film and it is associated with an increase in the oxidation level upon acidic treatment,[36] suppressing any residual polarons, and building bipolaron networks.[7] (Fig. 4c).

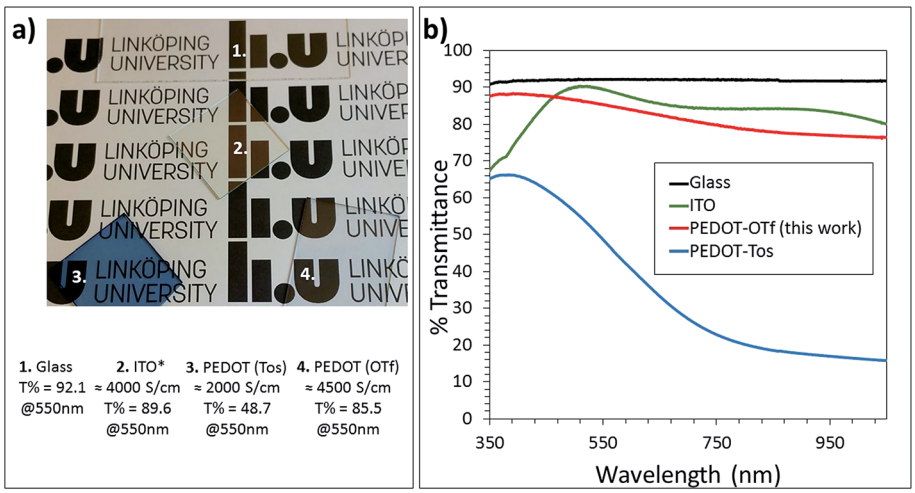

Fig. 3 Optimised thin films of the new PEDOT:OTf compared to glass, ITO and PEDOT:Tos films. (a) Photographs together with their relative conductivities and % transmittance at 550 nm and (b) UV-Vis spectra. *ITO conductivity from literature sources.[31,32]

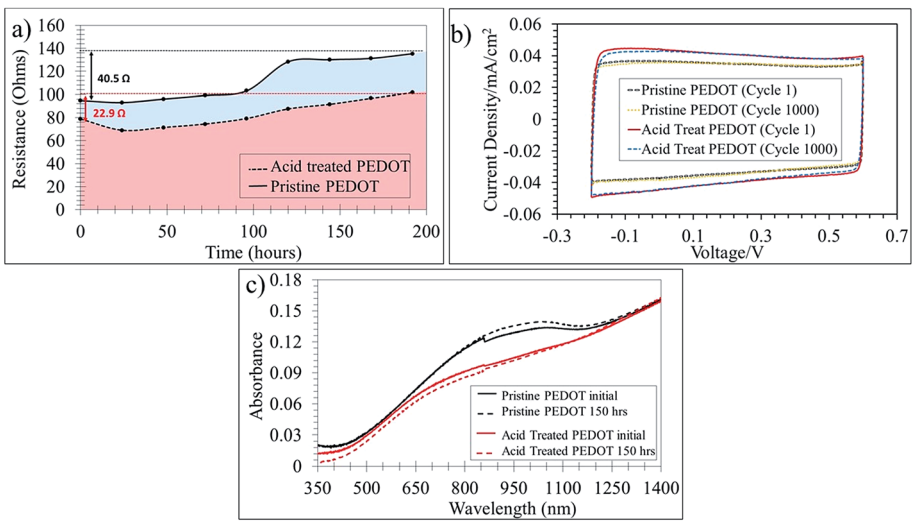

Fig. 4 (a) Stability of the pristine PEDOT:OTf and acid treated PEDOT:OTf films under ambient conditions, showing a steady increase in resistance over time. (b) Redox stability of pristine and acid treated PEDOT:OTf films over 1000 cycles between −0.2 and +0.6 V. (c) Optical investigation of the stability over 144 h from initial UV-Vis spectra observing only a minimal change in the optical properties.

Oxidation state

X-ray photoelectron spectroscopy (XPS) provides a convenient method to study the chemical environment of polymeric samples in thin film form. Within our system both the PEDOT and OTf molecules contain sulphur atoms in their chemical structure. However, the difference in binding energy allows the sulphur to be differentiated from the two molecules allowing the oxidation/doping level to be estimated from the S(2p) peaks within the XPS spectra. The S(2p) signal from one sulfur gives a doublet with a separation of 2 eV and an intensity ratio of 2 : 1; we will mention only the position of the main component of the doublet. The sulphur signal for PEDOT originates at 163.5 eV (Peak 1) with an asymmetric peak tail at higher binding energies corresponding to the positive charges present on the PEDOT chains which are partially delocalized on the sulphur atoms.[37] The main component of the second doublet at approximately 168 eV (Peak 3) corresponds to the Tof dopant molecule. The binding energy is higher than that of the sulfur in the thiophene ring because it is surrounded by three electronegative oxygen atoms on the sulfonate group. Note that the sulphur originating from the HSO_4^- anions inserted in the PEDOT film, upon acid treatment by ion exchange with the OTf anion, is assumed to overlap with the S(2p) signal of the OTf anion (Fig. 5b). The authors acknowledge that after acid treatment the PEDOT is doped with HSO_4^- anions rather than OTf anions but will be referred to as acid treated PEDOT–OTf for simplicity. The HSO_4^- anions lose their negative charge while coordinating with the positively charged PEDOT chains. The acid anion has previously been shown to replace the OTf anion using this acid treatment.[10] Using this information the oxidation level was calculated to be 25% and 32% for the pristine and acid treated PEDOT:OTf samples, respectively. This is in agreement with the acid treatment of PEDOT:Tos accompanied by an ion exchange and an increase in the oxidation level.[36]

The XPS results on the increased oxidation level in the case of the acid-treated PEDOT film partially justify the increased conductivity compared to the pristine PEDOT. However, the structure of the pristine and acid-treated films should be also investigated in order to fully understand the origins of this increase in conductivity of the acid treated film. Therefore, GIWAXS experiments have been carried out to analyse the structure of the pristine and acid treated PEDOT:OTf films.

GIWAXS and molecular modelling

The (q_r, q_z) wedge-corrected scattering images of the polymer films are shown in Fig. SI13,† while the corresponding 1D intensity *vs.* q scattering patterns are presented in (Fig. 6a). Despite the limitations in accessing the q-range below 0.4 $Å^{-1}$, a very intense diffraction peak is evident at $q^* = 0.45$ $Å^{-1}$, followed by a lower one at 0.9 $Å^{-1}$. The relative position of these peaks (q^*, $2q^*$) and their decreasing intensity suggest that they belong to the same family of reflections and that they correspond to an ordered lamellar structure. Following the interpretation by Aasmundtveit *et al.*,[38] we assign these peaks to the (h00) family of reflections of the PEDOT crystallites, the (h00) direction being perpendicular to the PEDOT backbone (c-axis) and along the EDOT plane direction. Therefore, the corresponding lattice size is $\alpha = 2\pi/q^* = 2\pi/q_{100} = 14.0$ Å. This size corresponds to that reported by Aasmundtveit *et al.*[38] for the distance between PEDOT chains along the α direction and with the counterions in between as depicted in Fig. 6e and f. Besides the (h00) family, a broad peak is present at around $q = 1.77$ $Å^{-1}$. It can be associated with diffraction that arises from a disordered π–π stacking. Therefore, it is assigned to the 020 peak[38] ($q_{\pi-\pi}$ in Fig. 6a). Note that the intensity of both the (100) and (020) peaks is higher in the case of the acid-treated film. Given the same dimensions and thicknesses of the two films, we conclude that the acid treatment results in more ordered films with higher crystallinity. This is the opposite as observed for PEDOT:Tos treated with HCl.[36] This suggests that the larger size of the SO_4^{2-}/HSO_4^- compared to the Cl^- is favourable because of its more similar size to the OTf anions. As a result, during the acid treatment the ion exchange $OTf^- \leftrightarrow HSO_4^-$ does not disrupt the molecular order obtained during the polymerization.

The experimental GIWAXS characterization of the pristine and acid treated films is consistent with the results of MD simulations when the X-ray diffraction pattern is obtained. The X-ray diffraction pattern and morphology of CPs are sensitive to the water content as experimentally shown for PEDOT:PSS[39] and theoretically demonstrated by MD simulations for PEDOT:TOS.[11] Thus, we obtained the X-ray diffraction pattern for each water evaporation step until matching the peak positions with the experimental 1D GIWAXS pattern, see Fig. SI14.† Fig. 6a

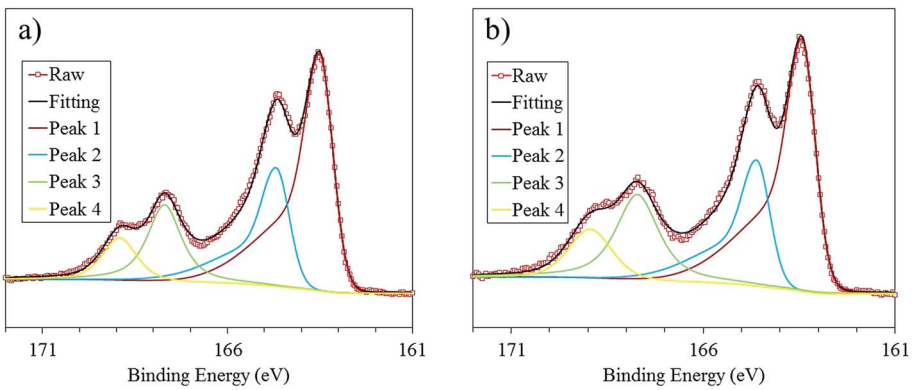

Fig. 5 XPS spectra and deconvolution of (a) pristine PEDOT:OTf and (b) acid treated PEDOT:OTf.

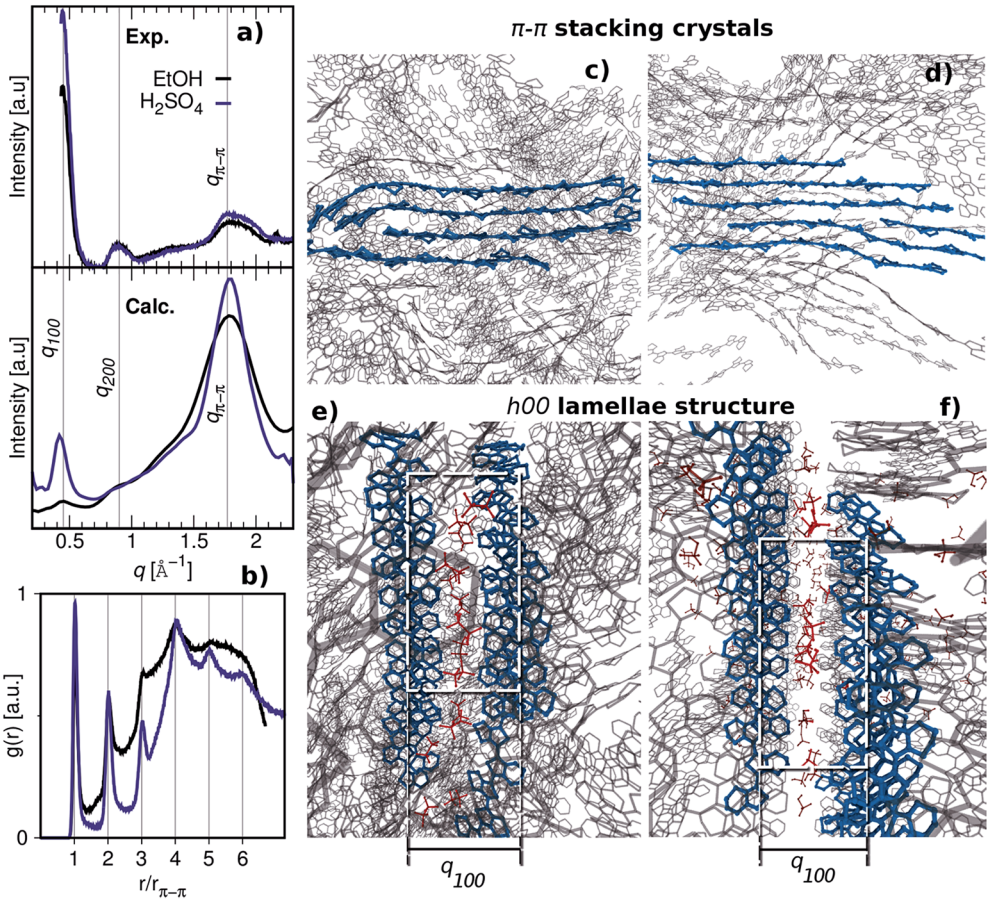

Fig. 6 (a) The experimental GIWAXS patterns and the calculated X-ray diffraction patterns of the pristine and the acid treated films. (b) Radial distribution function, $g(r)$, corresponding to the distance between the planes of PEDOT chains. (c)and (d) MD production snapshot where π–π stacking is shown for the pristine and acid treated films, respectively. (e) and (f) MD production snapshot where the lamellar structure is shown for the pristine and acid treated films, respectively. PEDOT chains are represented in blue. OTf and HSO_4^- counterions are represented in light tan. Solvent molecules are not shown. H atoms are not shown. Rectangular boxes in (e)and (f) show two neighbouring crystallites outlining the formation of the lamellar structure.

shows the calculated X-ray diffraction pattern of pristine and acid treated films, with a solvent content of 0 and 30 w/w %, respectively, for which the best agreement with the experimental patterns is obtained. In order to extract the crystallite size along the π–π direction, L_{020}, the Sherrer equation[40] is used for the experimental GIWAXS patterns,

$$L_{020} = 2\pi K/(\Delta q_{\pi-\pi}) \quad (3)$$

where $K \approx 0.93$ is the shape factor and $\Delta q_{\pi-\pi}$ is the full width at half maximum of the (020) peak. To extract $\Delta q_{\pi-\pi}$ the left side of the (020) peak was fitted to a Lorentz function, since its right side is associated with parasitic/background scattering, see Fig. 6a. The values of L_{020} obtained for the pristine and acid treated films are 20.5 and 22.1 Å respectively, and they correspond to 5.9 and 6.3 chains packed along the π–π stacking. This is confirmed by the calculation of the radial distribution functions, $g(r)$, corresponding to the distances between the planes of PEDOT chains in the MD simulations (Fig. 6b). For pristine and acid treated films the radial distribution $g(r)$ exhibits 5 and 6 $r/r_{\pi-\pi}$ peaks, respectively, that correspond to crystallites consisting of 6 and 7 chains. The MD snapshots that show the π–π crystallites formed in the pristine and acid treated films are demonstrated in Fig. 6c and d. It is noteworthy that the π–π crystallite sizes captured in the simulations are in good agreement with the calculated radial distribution functions and with the L_{020} sizes obtained using the experimental GIWAXS patterns.

Besides the good agreement between experiment and simulation regarding the (020) peak, the calculated diffraction patterns of the pristine and the acid treated films align well with the (h00) peaks located at $q \approx 0.45$ Å^{-1} and 0.90 Å^{-1}. As discussed above, these peaks are related to the formation of a lamellar structure along the α-axis (h00 direction). This lamellar structure is well apparent in Fig. 6e and f for the pristine and acid treated PEDOT:OTf films, respectively. The organization of the crystallites into lamellae is highlighted by dashed squares. According to these MD snapshots, two lamellae are separated by a lamellar d-spacing ≈ 14 Å, which corresponds well to the d-spacing that is calculated based on the (100) peak at $q \approx 0.45$ Å^{-1} from the calculated and experimental diffraction patterns (Fig. 6a). Moreover, the snapshots in Fig. 6e

and f reveal a higher disorder in the bulk of the film for the pristine film rather than for the acid treated film, consistent with the lower intensity of the (100) peaks that were recorded experimentally for the pristine film. The simulated systems do not take into account the effect of the substrate and thus the calculated X-ray diffraction patterns exhibit less order in the α-lattice direction with lower intensities for the (h00) peak families. This feature of the effect of the substrate is very well known for similar semiconducting polymers.[11,25] It is interesting to note that there is no observable shift in the diffraction peak between the HSO_4^- and the OTf anions since there is a van der Waals volume difference of 27% (Table SI1†). However, the projected radius for both minimal and maximal showed no significant difference, which corresponds to the radius of the projected 2D circular area (Table SI1†). Therefore, a diffraction peak shift may not appear in the spectra. The theoretical simulations presented above are a good indication that the increase in the experimental electrical conductivity of the acid-treated PEDOT:OTf films arises from an increase in crystallinity while still maintaining the π–π stacking.

Conclusion

Within this report, we have demonstrated the use of the oxidant species iron(III) trifluoromethane sulfonate with the vapour phase polymerization of EDOT. The optimization of the polymerization was achieved by investigating the components of the oxidant solution including a copolymer and the $Fe(OTf)_3$. The concentration of the oxidant, chemical nature of the solvent and polymerization conditions (temperature and time) were optimized to obtain an electrical conductivity as high as 3800 S cm^{-1}. After a post-treatment with H_2SO_4, the conductivity is further enhanced to 4500 S cm^{-1}. The electrical conductivity and optical transparency of the optimised PEDOT:OTf rivalled that of commercially transparent metal oxides with an acceptable electrochemical stability, thus suggesting their use as a transparent electrode in optoelectronic devices. XPS reveals that the acid treatment is accompanied by an increase in the oxidation level; which explains the positive effect on the conductivity as well as on the optical absorption in the visible region of the solar spectrum. The X-ray diffraction analysis supported by theoretical modelling indicates that the acid treatment with H_2SO_4 does not disturb the π–π stacking between the PEDOT chains. Hence, the higher oxidation level calculated through XPS and a higher order of crystallinity obtained by the acid treatment are deemed responsible for the higher conductivity measurements.

Conflicts of interest

There are no conflicts to declare.

Acknowledgements

This work was supported by the Knut and Alice Wallenberg Foundation (Project "The Tail of the Sun") and the Swedish Energy Agency (grant 38332-1). Computing was performed on resources provided by the Swedish National Infrastructure for Computing (SNIC) at NSC and HPC2N. The ESRF and NWO are acknowledged for allocating beam time at the Dutch-Belgian beamline (DUBBLE) for the GIWAXS experiments.

References

1 D. Kumar and R. C. Sharma, Advances in conductive polymers, *Eur. Polym. J.*, 1998, **34**(8), 1053–1060.
2 R. Brooke, P. Cottis, P. Talemi, M. Fabretto, P. Murphy and D. Evans, Recent advances in the synthesis of conducting polymers from the vapour phase, *Prog. Mater. Sci.*, 2017, **86**, 127–146.
3 R. Brooke, D. Evans, P. Hojati-Talemi, P. Murphy and M. Fabretto, Enhancing the morphology and electrochromic stability of polypyrrole via PEG–PPG–PEG templating in vapour phase polymerisation, *Eur. Polym. J.*, 2014, **51**, 28–36.
4 M. V. Fabretto, D. R. Evans, M. Mueller, K. Zuber, P. Hojati-Talemi, R. D. Short, *et al.*, Polymeric Material with Metal-Like Conductivity for Next Generation Organic Electronic Devices, *Chem. Mater.*, 2012, **24**(20), 3998–4003.
5 B. Winther-Jensen and K. West, Vapor-Phase Polymerization of 3,4-Ethylenedioxythiophene: A Route to Highly Conducting Polymer Surface Layers, *Macromolecules*, 2004, **37**(12), 4538–4543.
6 B. Winther-Jensen, D. W. Breiby and K. West, Base inhibited oxidative polymerization of 3,4-ethylenedioxythiophene with iron(III)tosylate, *Synth. Met.*, 2005, **152**(1), 1–4.
7 O. Bubnova, Z. U. Khan, H. Wang, S. Braun, D. R. Evans, M. Fabretto, *et al.*, Semi-metallic polymers, *Nat. Mater.*, 2013, **13**, 190.
8 B. Winther-Jensen, J. Chen, K. West and G. Wallace, Vapor Phase Polymerization of Pyrrole and Thiophene Using Iron(III) Sulfonates as Oxidizing Agents, *Macromolecules*, 2004, **37**(16), 5930–5935.
9 N. Massonnet, A. Carella, A. de Geyer, J. Faure-Vincent and J.-P. Simonato, Metallic behaviour of acid doped highly conductive polymers, *Chem. Sci.*, 2015, **6**(1), 412–417.
10 M. N. Gueye, A. Carella, N. Massonnet, E. Yvenou, S. Brenet, J. Faure-Vincent, *et al.*, Structure and Dopant Engineering in PEDOT Thin Films: Practical Tools for a Dramatic Conductivity Enhancement, *Chem. Mater.*, 2016, **28**(10), 3462–3468.
11 J. F. Franco-Gonzalez and I. V. Zozoulenko, Molecular Dynamics Study of Morphology of Doped PEDOT: From Solution to Dry Phase, *J. Phys. Chem. B*, 2017, **121**(16), 4299–4307.
12 S. Rudd, J. F. Franco-Gonzalez, S. Kumar Singh, Z. Ullah Khan, X. Crispin, J. W. Andreasen, *et al.*, Charge transport and structure in semimetallic polymers, *J. Polym. Sci., Part B: Polym. Phys.*, 2018, **56**(1), 97–104.
13 R. Brooke, M. Fabretto, M. Krasowska, P. Talemi, S. Pering, P. J. Murphy, *et al.*, Organic energy devices from ionic liquids and conducting polymers, *J. Mater. Chem. C*, 2016, **4**(7), 1550–1556.

14 M. Fabretto, M. Müller, K. Zuber and P. Murphy, Influence of PEG-ran-PPG Surfactant on Vapour Phase Polymerised PEDOT Thin Films, *Macromol. Rapid Commun.*, 2009, **30**(21), 1846–1851.

15 I. Horcas, R. Fernández, J. M. Gómez-Rodríguez, J. Colchero, J. Gómez-Herrero and A. M. Baro, WSXM: A software for scanning probe microscopy and a tool for nanotechnology, *Rev. Sci. Instrum.*, 2007, **78**(1), 013705.

16 S. Plimpton, Fast Parallel Algorithms for Short-Range Molecular Dynamics, *J. Comput. Phys.*, 1995, **117**(1), 1–19.

17 J. Wang, R. M. Wolf, J. W. Caldwell, P. A. Kollman and D. A. Case, Development and testing of a general amber force field, *J. Comput. Chem.*, 2004, **25**(9), 1157–1174.

18 A. I. Jewett, Z. Zhuang and J.-E. Shea, Moltemplate a Coarse-Grained Model Assembly Tool, *Biophys. J.*, 2013, **104**(2), 169a.

19 H. J. C. Berendsen, J. P. M. Postma, W. F. van Gunsteren and J. Hermans, Interaction Models for Water in Relation to Protein Hydration, in *Intermolecular Forces: Proceedings of the Fourteenth Jerusalem Symposium on Quantum Chemistry and Biochemistry Held in Jerusalem, Israel, April 13–16, 1981*, ed. B. Pullman, Springer, Dordrecht, Netherlands, 1981, pp. 331–342.

20 A. Elshchner, S. Kirchmeyer, W. Lovenich, U. Merker and K. Reuter, *PEDOT: Principles And Applications Of An Intrinsically Conductive Polymer*, 2011.

21 Y.-S. Lin, G.-D. Li, S.-P. Mao and J.-D. Chai, Long-Range Corrected Hybrid Density Functionals with Improved Dispersion Corrections, *J. Chem. Theory Comput.*, 2013, **9**(1), 263–272.

22 R. Krishnan, J. S. Binkley, R. Seeger and J. A. Pople, Self-consistent molecular orbital methods. XX. A basis set for correlated wave functions, *J. Chem. Phys.*, 1980, **72**(1), 650–654.

23 M. J. Frisch, G. W. Trucks, H. B. Schlegel, G. E. Scuseria, M. A. Robb, J. R. Cheeseman, G. Scalmani, V. Barone, G. A. Petersson, H. Nakatsuji, X. Li, M. Caricato, A. V. Marenich, J. Bloino, B. G. Janesko, R. Gomperts, B. Mennucci, H. P. Hratchian, J. V. Ortiz, A. F. Izmaylov, J. L. Sonnenberg, D. Williams-Young, F. Ding, F. Lipparini, F. Egidi, J. Goings, B. Peng, A. Petrone, T. Henderson, D. Ranasinghe, V. G. Zakrzewski, J. Gao, N. Rega, *et al.*, Guassian Ink., Wallingford CT, 2016.

24 U. C. Singh and P. A. Kollman, An approach to computing electrostatic charges for molecules, *J. Comput. Chem.*, 1984, **5**(2), 129–145.

25 J. F. Franco-Gonzalez, E. Pavlopoulou, E. Stavrinidou, R. Gabrielsson, D. T. Simon, M. Berggren, *et al.*, Morphology of a self-doped conducting oligomer for green energy applications, *Nanoscale*, 2017, **9**(36), 13717–13724.

26 W. Shinoda, M. Shiga and M. Mikami, Rapid estimation of elastic constants by molecular dynamics simulation under constant stress, *Phys. Rev. B*, 2004, **69**(13), 134103.

27 M. E. Tukerman, J. Alejandre, R. Lopez-Rendon, A. L. Jochim and G. J. Martyna, Liouville-operator derived measure-preserving integrator for molecular dynamics simulations in the isothermal–isobaric ensemble, *J. Phys. A: Math. Gen.*, 2006, **39**(19), 5629.

28 L. Capolungo, S. P. Coleman and D. E. Spearot, Virtual diffraction analysis of Ni [0 1 0] symmetric tilt grain boundaries, *Modell. Simul. Mater. Sci. Eng.*, 2013, **21**(5), 055020.

29 W. Bras, I. P. Dolbnya, D. Detollenaere, R. Van Tol, M. Malfois, G. N. Greaves, *et al.*, Recent experiments on a small-angle/wide-angle X-ray scattering beam line at the ESRF, *J. Appl. Crystallogr.*, 2004, **36**(3–1), 791–794.

30 R. Brooke, D. Evans, M. Dienel, P. Hojati-Talemi, P. Murphy and M. Fabretto, Inkjet printing and vapor phase polymerization: patterned conductive PEDOT for electronic applications, *J. Mater. Chem. C*, 2013, **1**(20), 3353–3358.

31 J. Ouyang, C. W. Chu, F. C. Chen, Q. Xu and Y. Yang, High-Conductivity Poly(3,4-ethylenedioxythiophene):Poly(styrene sulfonate) Film and Its Application in Polymer Optoelectronic Devices, *Adv. Funct. Mater.*, 2005, **15**(2), 203–208.

32 J. Ni, H. Yan, A. Wang, Y. Yang, C. L. Stern, A. W. Metz, *et al.*, MOCVD-Derived Highly Transparent, Conductive Zinc- and Tin-Doped Indium Oxide Thin Films: Precursor Synthesis, Metastable Phase Film Growth and Characterization, and Application as Anodes in Polymer Light-Emitting Diodes, *J. Am. Chem. Soc.*, 2005, **127**(15), 5613–5624.

33 P. Hojati-Talemi, C. Bächler, M. Fabretto, P. Murphy and D. Evans, Ultrathin Polymer Films for Transparent Electrode Applications Prepared by Controlled Nucleation, *ACS Appl. Mater. Interfaces*, 2013, **5**(22), 11654–11660.

34 R. Brooke, M. Fabretto, N. Vucaj, K. Zuber, E. Switalska, L. Reeks, P. Murphy and D. Evans, Effect of oxidant on the performance of conductive polymer films prepared by vacuum vapor phase polymerization for smart window applications, *Smart Mater. Struct.*, 2015, **24**(3), 035016.

35 R. Brooke, M. Fabretto, P. Hojati-Talemi, P. Murphy and D. Evans, Evidence for 'bottom up' growth during vapor phase polymerization of conducting polymers, *Polymer*, 2014, **55**(16), 3458–3460.

36 Z. U. Khan, O. Bubnova, M. J. Jafari, R. Brooke, X. Liu, R. Gabrielsson, *et al.*, Acido-basic control of the thermoelectric properties of poly(3,4-ethylenedioxythiophene)tosylate (PEDOT-Tos) thin films, *J. Mater. Chem. C*, 2015, **3**(40), 10616–10623.

37 G. Zotti, S. Zecchin, G. Schiavon, F. Louwet, L. Groenendaal, X. Crispin, *et al.*, Electrochemical and XPS Studies toward the Role of Monomeric and Polymeric Sulfonate Counterions in the Synthesis, Composition, and Properties of Poly(3,4-ethylenedioxythiophene), *Macromolecules*, 2003, **36**(9), 3337–3344.

38 K. E. Aasmundtveit, E. J. Samuelsen, L. A. A. Pettersson, O. Inganäs, T. Johansson and R. Feidenhans'l, Structure of thin films of poly(3,4-ethylenedioxythiophene), *Synth. Met.*, 1999, **101**(1), 561–564.

39 C. M. Palumbiny, F. Liu, T. P. Russell, A. Hexemer, C. Wang and P. Müller-Buschbaum, The Crystallization of PEDOT:PSS Polymeric Electrodes Probed In Situ during Printing, *Adv. Mater.*, 2015, **27**(22), 3391–3397.

40 D.-M. Smilgies, Scherrer grain-size analysis adapted to grazing-incidence scattering with area detectors, *J. Appl. Crystallogr.*, 2009, **42**(Pt 6), 1030–1034.

